RSC Advances

PAPER

Cite this: *RSC Adv.*, 2021, **11**, 31583

Molecular insight into carbon dioxide hydrate formation from saline solution

Chanjuan Liu,[abcd] Xuebing Zhou[abcd] and Deqing Liang *[abcd]

Received 23rd May 2021
Accepted 15th September 2021

DOI: 10.1039/d1ra04015d

rsc.li/rsc-advances

Carbon dioxide hydrate has been intensively investigated in recent years because of its potential use as gas and heat storage materials. To understand the hydrate formation mechanisms, the crystallization of CO_2 hydrate from NaCl solutions was simulated at a molecular level. The influence of temperature, pressure, salt concentration and CO_2 concentration on CO_2 hydrate formation was evaluated. Results showed that the amount of the newly formed hydrate cages pressure went through a fast linear growth period followed by a relatively stable period. Pressure had little effect on CO_2 hydrate formation and temperature had a significant influence. The linear growth rate was greatly reduced as the temperature dropped from 255 to 235 K. The salt ion pairs could inhibit CO_2 hydrate formation, suggesting that we should choose the lower salinity areas if we want to storage CO_2 as gas hydrates in the seabed sediments. The observations in this study can provide theoretical support for the micro mechanism of hydrate formation, and provide a theoretical reference for the technology of hydrate based CO_2 storage.

1. Introduction

Gas hydrates are ice-like compounds that form through a combination of gas and water molecules. Under elevated pressure and low temperature, water molecules form a cage-like host framework connected by hydrogen bonds and gas molecules are trapped inside as guests. The structure of gas hydrate largely depends on the size of the gas molecules.[1,2] For example, methane (CH_4), carbon dioxide (CO_2) and ethane form sI hydrates; propane, nitrogen and tetrahydrofuran form sII hydrates.[3] Naturally occurring gas hydrates, mainly CH_4 hydrate, are considered as a potential alternative energy due to their huge reserves and wide distribution.[4,5] More than 230 gas hydrate deposits have been detected worldwide and the amount of carbon stored in natural gas hydrates is estimated to be twice that of all the other carbon sources combined.[6] At the same time, CO_2 hydrates are found to be an eco-friendly material for CO_2 storage.[7–9] Thermodynamic calculations show that CO_2 can be stably preserved in the seabed where the water depth is around 250 to 530 m which is more stable in the hydrate phase than CH_4 at relevant pressures.[10] Therefore, CO_2 is suggested to displace CH_4 from hydrate phase, releasing CH_4 and capturing CO_2 in the hydrate bearing sediments, which is expected to impact on both the sustainability of energy system and the global climate change.[11–13]

The gas exchange concept for natural gas production has been confirmed viable technically. In 2011 and 2012, the field test conducted at the Alaska North Slope tried to replace CH_4 with a gas mixture of 23 mol% CO_2 and 77 mol% N_2 from hydrate reservoir and found that a total of 24410 m^3 of CH_4 was recovered by sequestrating 2247 m^3 of N_2–CO_2 mixtures successfully within 48 days.[14] This field test reveals that the gas exchange in hydrate phase is a slow process and is limited by a series of factors. Then revealing the kinetic mechanism and key factors affecting gas exchange become a hotspot in gas hydrate research.[15–18] With the recent progress in learning the kinetic features of CH_4–CO_2 replacement, gas exchange in hydrate phase was found to start with a fast reaction from simple hydrate to mixed hydrate at hydrate surface, then the gas replacement proceeds towards the deep inside of hydrate phase where gas diffusion is limited by the break of hydrate cages.[19,20] However, there is a discrepancy lie in the existence of free water molecules in gas exchange. Ota *et al.*[21,22] built a kinetic model by assuming that CH_4–CO_2 exchange in hydrate phase consist of a series of dissociation and reformation processes. This model provides a well description of the gas exchange in the initial stage and widely used.[13,23,24] However, such an assumption is not supported from microscopic level. Magnetic resonance imaging (MRI) and differential scanning calorimeter (DSC) revealed that there was no sign of free water molecules appeared during gas replacement.[25–27] Therefore, the gas exchange is suggested to proceed without significant change to host water lattice.

Molecular dynamic (MD) simulation is an effective tool to study the microscopic behavior of gas hydrate and has been widely used to study the kinetic process of gas hydrate.[28–34] However, a direct simulation on the gas exchange at hydrate surface lead to different results because of the deviation in

[a]*Chinese Acad Sci, Guangzhou Ctr Gas Hydrate Res, Guangzhou Inst Energy Convers, Guangzhou 510640, Peoples R China. E-mail: liangdq@ms.giec.ac.cn*
[b]*CAS Key Lab Gas Hydrate, Guangzhou 510640, Peoples R China*
[c]*Guangdong Prov Key Lab New & Renewable Energy Res, Guangzhou 510640, Peoples R China*
[d]*State Key Lab Nat Gas Hydrate, Beijing 100028, China*

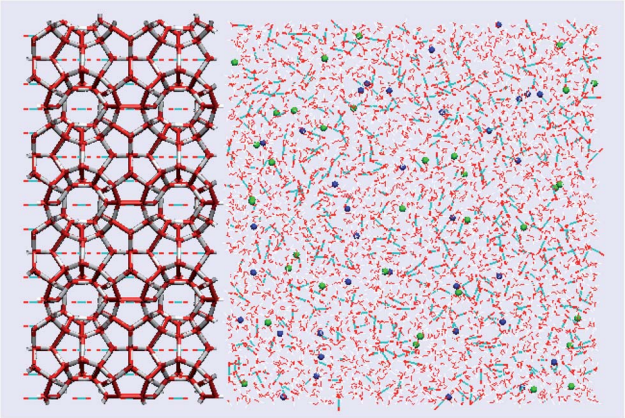

Fig. 1 Snapshot of the typical initial configuration in this study. There are 2 × 4 × 4 unit CO_2 hydrate in the left side, and the saline solution of CO_2 in the right side. The rod structures are CO_2, the red balls are O, the blue balls are Na^+, and the green balls are Cl^-.

computational methods. Liu *et al.*[35] and Tung *et al.*[36] reported that the host lattice was slightly distorted during CH_4–CO_2 exchange. While Bai *et al.*[37] and Wu *et al.*[38] revealed that the CH_4–CO_2 exchange pathway started with the melting of CH_4 hydrate near hydrate surface and followed by the formation of an amorphous CO_2 hydrate layer. Since the CH_4–CO_2 exchange is closely related to the CH_4 dissociation and the CO_2 hydrate formation, it will be necessary to characterize the formation and dissociation of gas hydrate individually. Sarupria *et al.*[39] found that CO_2 hydrate dissociation rate was dependent on the fractional occupancy of each cage type. Qi *et al.*[40] revealed that gas hydrates was not salt-free and massive salt ions may concentrate on the surface of the hydrates. Yi *et al.*[41] noted that NaCl and $MgCl_2$ decreased the mobility of their surrounding water molecules and inhibited CO_2 hydrate growth. He *et al.*[42] suggested that absorbing sufficient CO_2 molecules around the CO_2 hydration shells and a high aqueous CO_2 concentration were the key factors governing the CO_2 hydrate nucleation.

Since the CO_2 hydrate formation is closely related to the CH_4–CO_2 exchange in hydrate phase, CO_2 hydrate crystallization from NaCl solution was characterized from molecular level in this work. The growth pattern of hydrate cage at the hydrate–liquid interface was recorded. The influence of temperature (235–275 K), pressure (30–100 MPa) and salt concentration (0–20 wt%) on the growth rate of CO_2 hydrate was measured. Results of this work is useful to identify the kinetic properties of CO_2 hydrate formation from molecular level.

2. Simulation details

2.1 Simulation models and force field

The initial system is a solid–liquid model with the sizes of 73 × 48 × 48 Å^3, which include hydrate phase and liquid phase as seen in Fig. 1. The hydrate phase consists of a 2 × 4 × 4 unit cell of sI hydrate structure with CO_2 molecules full occupying the hydrate cages. The liquid water phase contains 2944 water molecules, 512 CO_2 molecules and a certain amount of sodium chloride ion pairs determined by experimental conditions. MD simulations were performed in the GROMACS software package. The TIP4P/2005 model was used to describe water molecules in liquid phase.[43] Zhang model was employed for CO_2 molecules, which was better in predicting the self-diffusion at low temperature.[44] The potential parameters of water and CO_2 molecule used in this work were listed in Table 1.

The pair additive Lennard–Jones potential model in association with the coulombic charge expression isemployed for non-bonded interactions which can be written in following form the cross interactions between water and guest molecules were calculated according to the Lorentz–Berthelot combining rules[45] *via*.

$$E(r_{ij}) = \sum_i \sum_j \left\{ \frac{q_i q_j}{r_{ij}} + 4\varepsilon_{ij} \left[\left(\frac{\sigma_{ij}}{r_{ij}} \right)^{12} - \left(\frac{\sigma_{ij}}{r_{ij}} \right)^{6} \right] \right\} \quad (1)$$

$$\sigma_{ij} = \frac{1}{2}(\sigma_{ii} + \sigma_{jj}) \quad (2)$$

$$\varepsilon_{ij} = (\varepsilon_{ii}\varepsilon_{jj})^{1/2} \quad (3)$$

where σ and ε are the Lennard–Jones interaction parameters.

In this paper, all the simulations were performed by the NPT ensemble. The temperature was coupled by the Nosé–Hoover thermostat with a period constant of 1.0 ps and the pressure was coupled by the Parrinello-Rahman barostat with a period constant of 1.0 ps. In each simulation, energy minimization was initially performed to relax the initial configuration with the steepest descent algorithm. After energy minimization, the system was equilibrated in the NVT ensemble at 255 K, and then the NPT ensemble was set with a temperature of 255 K and a pressure of 30 MPa. The cutoff distance was 10 Å for the Lennard–Jones potential. Periodic boundary conditions were used in all three directions[46] and the long-range electrostatic interactions were calculated using the particle mesh Ewald (PME) method with a real space cutoff of 10 Å, spline order of 4, and Fourier spacing of 1.2 Å.[47]

Table 1 Interaction parameters for H_2O and CO_2

Molecule	Atom/site	σ_{ii} (Å)	ε_{ii} (KJ/Mol)	q (e)	l^b (Å)	α^c (°)
—	O	3.1589	0.774 912	0.0	$l_{OH} = 0.9572$	∠HOH = 104.52
H_2O	H	0	0	0.5564	—	—
	M[a]	0	0	−1.1128	—	—
CO_2	C	2.7918	0.239832	0.5888	$l_{CO} = 1.163$	∠OCO = 180
—	O	3.0	0.687244	−0.2944	—	—

[a] The site M of H_2O lies in the molecular plane on the bisector of the H–O–H angle, and the distance between atom O and M is 0.1546 Å. [b] l refers to the bond length. [c] α refers to the bond angle.

2.2 Data analysis

The face-saturated incomplete cage analysis method (FSICA) was used to recognize all the face-saturated cages in the system.[48] For a standard polyhedron, the cage with both face saturated and edge saturated could be defined as a complete cage (CC). Here, the face saturated means that each edge of a cage is shared by two and only two faces which are water rings that no more than six members. The edge saturated means that each vertex in the polyhedron is shared by three edges at least. In brief, the face-saturated cages include face-saturated complete cages (FSCC) such as 5^{12} (D-cage), $5^{12}6^2$ cage (T-cage), $5^{12}6^3$, $4^15^{10}6^2$, $4^15^{10}6^3$ and $5^{12}6^4$ cages and face-saturated incomplete cages (FSIC) such as $[5^26^3]_5$ and $[5^26^4]_5$ cages. In this study, CO_2 hydrate was SI hydrate, composed of D cage and T cage. The 5^{12} cage (D-cage) means that the cage has twelve pentagonal faces and the 5^{12} 6^2 cage (T-cage) means that the cage has ten pentagonal faces and two hexagonal faces. We can see the snapshots of 5^{12}, $5^{12}6^2$, and $5^{12}6^3$ cages in Fig. 2.

Each cage face had an adsorption site, which was along the normal vector crossing the face center and was 3 Å away from the center. The CH_4 or CO_2 molecules were identified as adsorbed, guest or free molecules. The linkages between each two hydrate cages through a cage face were classified into structure I (sI) links, structure II (sII) links, and structure H (sH) links. The linkage between a D-cage and a T-cage was recognized as an sI link because such linkage only existed in the sI hydrate structures, whereas the linkage between two D-cages could be either sII or sH.

We also used a four body order parameter (F_4) to analyze the arrangement of H_2O molecules. The F_4 is defined as follow

$$F_4 = \frac{1}{n}\sum_{i=0}^{n}\cos 3\phi_i \quad (4)$$

where ϕ_i is the torsion angle for two adjacent water molecules,[49] the average values of F_4 for ice, liquid water, and hydrate are −0.4, −0.04, and 0.7, respectively.

3. Results

3.1. The effect of pressure

To evaluate pressure effect, CO_2 hydrates were allowed to grow at 30 MPa, 50 MPa and 100 MPa from the NaCl solution with a fixed initial NaCl concentration of 3.5 wt%. The growth rates of hydrate cages are shown in Fig. 3. The amount of the newly formed D-cages and T-cages were found to grow simultaneously once the simulation started and reached stable after 800 ns.

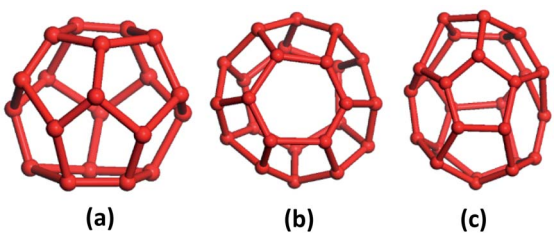

Fig. 2 The snapshots of cages. (a) D-Cage (5^{12}), (b) T-cage ($5^{12}6^2$), (c) $5^{12}6^3$ cage.

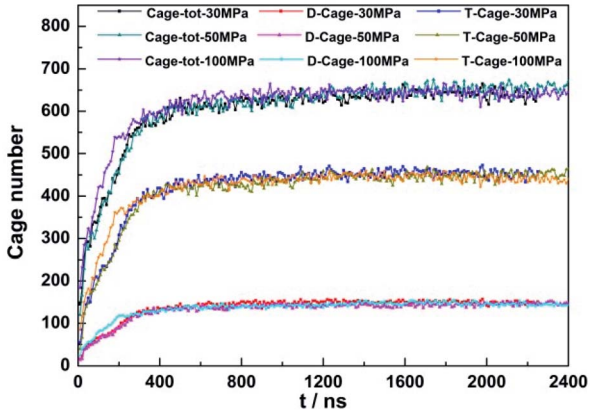

Fig. 3 The amount of newly formed D-cage and T-cage during CO_2 hydrate growth at 255 K.

In the initial 800 ns of hydrate growth, the amount of newly formed D- and T-cage increase in generally the same profile when the pressure was 30 and 50 MPa. As the pressure increased up to 100 MPa, the amount of newly formed D- and T-cage were found to grow faster during the initial 300 ns, then followed the same trend as those at 30 and 50 MPa, suggesting that the pressure increase from 30 to 100 MPa had limited promotion effect on the growth of hydrate crystal. Such a result agreed well with previous work, but was contradict with the conclusion that the hydrate growth rate was linearly correlated with gas fugacity difference between hydrate and gas phases which is frequently defined as driving force of hydrate growth.[50,51] It should be noted that such a linear relationship between hydrate growth rate and driving force was got from macroscopic measurements where hydrate crystals grew with a continuous increase in amount of crystals in bulk liquid phase. Therefore, pressure increase was assumed to boost the formation of hydrate nuclei rather than the growth of an individual crystal.

In the simulation after 800 ns, the amount of the newly formed T-cages was about 3 times that of D-cages which was consistent with the ratio of T- and D-cage in a typical crystal unit of sI hydrate, suggesting that the hydrate grew as a complete crystal unit which was not influenced by pressure.

3.2. The effect of temperature

The temperature effect on CO_2 hydrate growth were carried out in a system with fixed initial NaCl concentration of 3.5 wt% and pressure at 30 Mpa while the temperature was controlled at 235, 255 and 275 K. The profiles of the newly formed D- and T-cages at different temperature were shown in Fig. 4.

As the temperature decreased from 255 to 235 K, the ratio of newly formed T- and D-cages was found to keep around 3.0 throughout each simulation, but the growth patterns of the newly formed cages changed. At 255 K, both the D- and T-cages grew linearly in the first 400 ns and reached stable thereafter. However, the linearly growth lasted only about 150 ns when the temperature decreased down to 235 K, and then the amount of both cages grew slowly and continuously in the next 2000 ns.

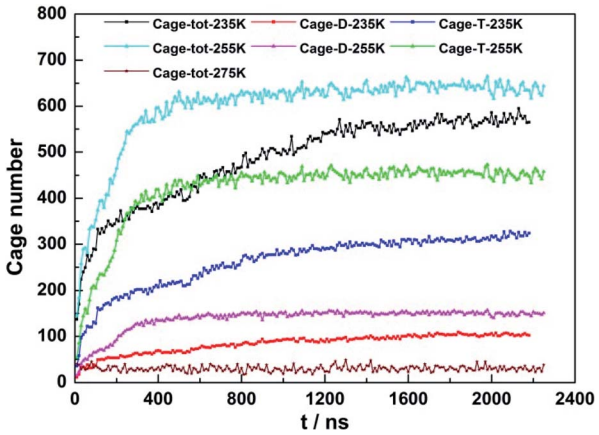

Fig. 4 The amount of newly formed D-cage and T-cage with an initial pressure of 30 MPa.

Although a temperature decrease could gain an increase in driving force at fixed initial pressure, the initial hydrate growth was not found to be faster at lower temperature. In this case, lowering temperature is not beneficial to hydrate crystallization. From another perspective, the water molecules activity that determined largely by temperature was suggested to be more important than the gas diffusivity that affected by pressure in formation of cages on hydrate crystal surface.

3.3. The effect of NaCl concentration

The effect of NaCl concentration on CO_2 hydrate growth was measured at 30 MPa, 255 K with a NaCl concentration range from 0 to 20 wt%. The amount of the newly formed D- and T-cages during the simulation at different NaCl concentration was shown in Fig. 5. The amount of hydrate cages went through a linear growth in the initial stage and reached stable thereafter, which was not affected by the salt concentration.

At fixed initial thermodynamic conditions, increasing NaCl concentration would impair the stability of CO_2 hydrates and was suggested to reduce the CO_2 hydrate formation rate.[52] As expected, the amount of D-cage and T-cage grown from pure water got the highest linear growth rate at the initial stage and the total amount of the newly formed cages was also higher than the systems containing NaCl. We can see that during the first 400 nanoseconds of growth, with the NaCl concentration increased from 3.5 to 20 wt%, the growth rate of CO2 hydrate decreases slightly, and the total number of cages formed decreases, but such a decrease was not evident.

In the process of the carbon dioxide hydrate growth, the $5^{12}6^2$ cage and 5^{12} cage number ratio was slightly above 3 : 1 when the system reached stable as seen in Fig. 6. However, the T/D cage ratio was much higher at the initial stage, which was around 3.6 in maximum, suggesting that the $5^{12}6^2$ cages formed first and faster than the 5^{12} cages. At the same time we analyzed the influence of the NaCl concentration on the T/D cage ratio, and found that its ratio was just reached 3.2 and then stable at about 3 in the pure water system, while added NaCl, the T/D cage ratio could reach 3.6 in maximum. The higher the NaCl concentration, the larger the T/D cage ratio. It was suggested that the NaCl solution would inhibit the D cage's growth. We also observed a carbon dioxide bubbles generated in the process of formation while concentration was set to 7% and 20%.

Fig. 7 shows the changes of cages in the process of CO_2 hydrate formation when the concentration of salt solution is 0 and 3.5 wt%, the formation of the simulation time is 1 microsecond. Furthermore, in the process of the carbon dioxide hydrate formation, we observed that it can form not only 5^{12} and $5^{12}6^2$ cages, but also form $5^{12}6^3$ cages, which are shown in yellow in Fig. 6. The $5^{12}6^3$ cages are not the components of SI, SII and SH hydrates, but can form in the process of gas hydrate formation, which occupied a large mount.[48] This means that the $5^{12}6^3$ cage is a middle cage type, it can be turned into $5^{12}6^2$ or $5^{12}6^4$ cage. In the process of simulations, we tracked the salt ions activity, and found that no salt ions getting into the water cages. This is because the salt ions with charges, they will be excluded from the cage while they come close to the cage.

In addition, we analysed the four body order parameter (F_4) of CO_2 hydrate formation under different concentrations as

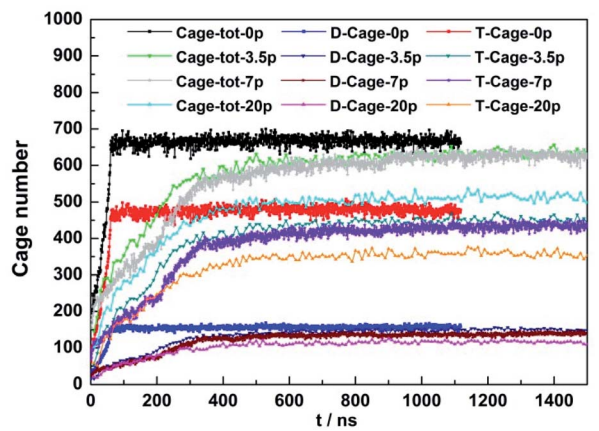

Fig. 5 The amount of D-cage and T-cage formed from different NaCl concentration at 255 K, 30 MPa.

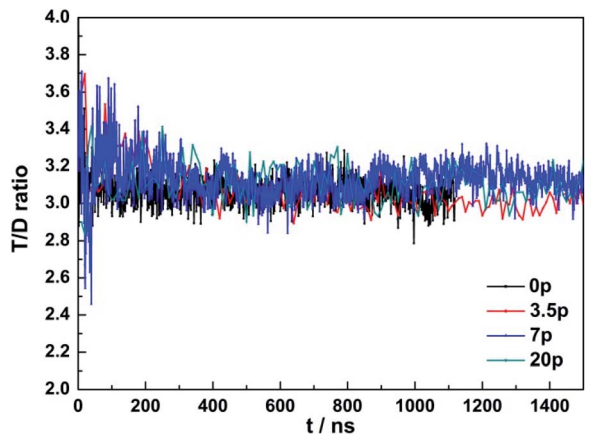

Fig. 6 The rate change of T-cage and D-cage during carbon dioxide hydrate formation.

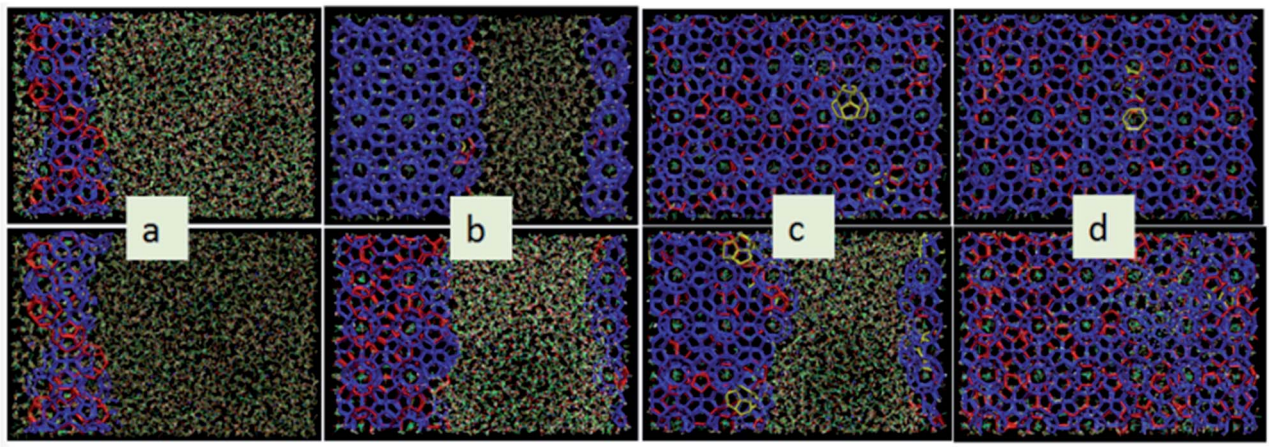

Fig. 7 The cage changes in the process of CO2 hydrate formation. The above is pure carbon dioxide hydrate, and the below is carbon dioxide hydrate with 3.5% concentration of NaCl. The red cages are 512 cages, blue cages are 51262 cages, and the yellow cages are 51263 cages. (a) shows the state of initial computation time after time relaxation, (b) shows the simulation time of 50 ns, (c) shows 100 ns and (d) shows 1000 ns.

seen in Fig. 8. The pure CO_2 and water solution (the black line) formed carbon dioxide hydrate fast and the F_4 value was closer to 0.7, which indicated that carbon dioxide hydrate under pure carbon dioxide aqueous solution had a higher crystallinity. With the increase of concentration of salt solution, the rate of hydrate formation gradually reduced, and the formation of hydrate crystals decreased. This result shown that salt ions inhibited the formation and growth of hydrates, and the sodium chloride was an inhibitor. This was also consistent with the experimental results by Andreas S. Braeuer.[53]

3.4 The effect of CO_2 concentration

The CO_2 concentration on CO_2 hydrate formation was also taken into consideration in this work. Although CO_2 shows much higher solubility than CH_4, the nucleation of CO_2 hydrate requires a much higher critical concentration. The observed critical concentration for CO_2 hydrate nucleation was 0.08 in mole fraction[42] while the guest concentration critical concentration for CO_2 hydrate nucleation was just 0.04 in mole fraction.[54] And they found that if the concentration in the solution under this number, it would nucleate hydrate very hardly.[55] So in this paper, in order to analyse how the carbon dioxide concentration affects carbon dioxide hydrate formation. We selected a perfect crystalline mole concentration 0.148 and one concentration can form carbon dioxide hydrate which is 0.1. The F_4 parameter of the different mole fraction in Fig. 9. We can see that almost all the carbon dioxide solution formed hydrates when the mole fraction was 0.148, and the F_4 parameter value is about to 0.7, but the 0.1 mole fraction solution formed slowly and could not formed completely, and the F_4 parameter value is just upon 0.4. This means that the higher the carbon dioxide concentration in water, the easier the carbon dioxide hydrate formed, and the higher the cage crystallinity.

The final state of different mole concentration was shown in Fig. 10. The formation of the simulation time of 0.148 mole concentration solution is 1 microsecond while the simulation time of 0.1 mole concentration solution is 1.5 microsecond. The study found

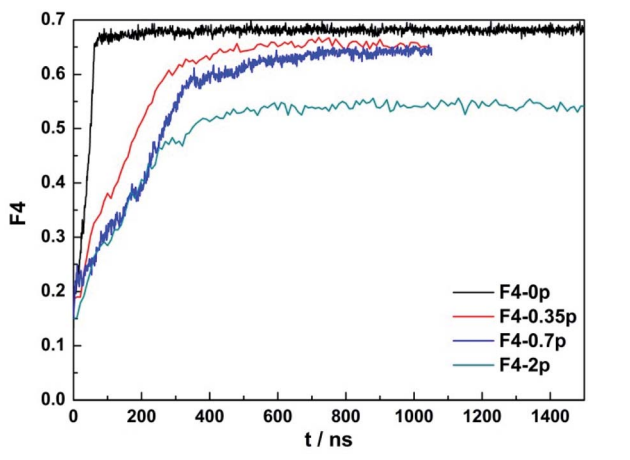

Fig. 8 The F_4 parameter of CO_2 hydrate system with different concentration salt solution.

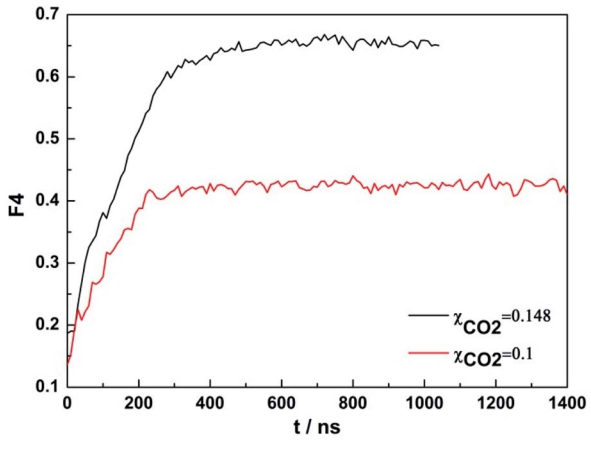

Fig. 9 The F_4 parameter of CO_2 hydrate with different CO_2 mole fraction in water. The black line of the mole fraction was 0.148 and the red line is 0.1.

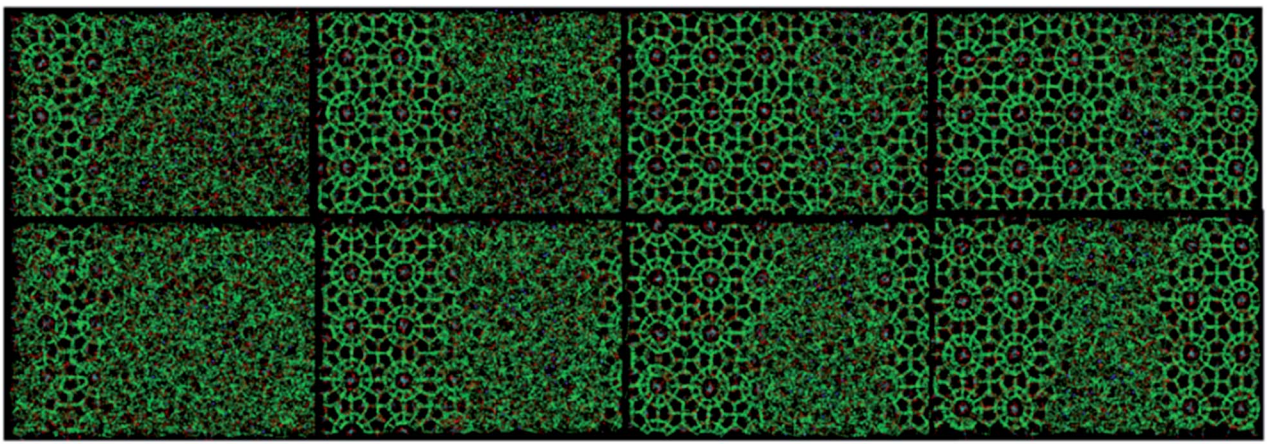

Fig. 10 The carbon dioxide hydrate formation of different CO_2 concentration. The above one shows carbon dioxide mole fraction is 0.148 and the below one shows the mole fraction is 0.1. From left to right, the simulation time is the state of initial computation time after time relaxation, 100 ns, 500 ns and 1500 ns in turn.

that with CO_2 hydrate formed, CO_2 molecules occupied the T and D cages, the concentration of CO_2 solution reduced, and then the growth of hydrate speed decreased. It was also suggested that low concentration of CO_2 solution was hard to continue to form hydrate.

4. Conclusions

In this paper, we analyzed the effects of temperature and pressure on the formation of CO_2 hydrate. It is found that pressure has little effect on the formation of CO_2 hydrate, while temperature has a great effect under the condition of CO_2 hydrate can form. The formation rate of CO_2 hydrate increased with the decrease of temperature. We compared the different concentrations of salt solution on CO_2 hydrate formation, and found that the higher the salt concentration, the slower the CO_2 hydrate formation. During the process of the CO_2 hydrate formation, it can form $5^{12}6^3$ cage and $5^{12}6^3$ cage will turn into $5^{12}6^2$ or $5^{12}6^4$ cage. The 5^{12} cage and $5^{12}6^2$ cage number ratio is about 1 : 3 in the process of carbon dioxide hydrate formation, this is the ratio of sI hydrate. During the formation of CO_2 hydrate, salt ions could not enter the cage or be absorbed on the cage face. This suggests that salt ions inhibit the formation and growth of hydrates. At the same time, we studied the influence of different CO_2 mole concentration on CO_2 hydrate formation, and found that the higher the CO_2 mole fraction in water, the faster the CO_2 hydrate formed, and the higher the cage crystallinity. The results provide theoretical support for the micro mechanism of hydrate formation, and provide a theoretical reference for the technology of hydrate storing CO_2.

Conflicts of interest

The authors declare no competing financial interest.

Acknowledgements

We thank the national supercomputing center in Shenzhen for the allocation of computer time. This work is supported by National Natural Science Foundation of China (41603062, 51706230).

References

1 Z. X. Huo, K. Hester, E. D. Sloan and K. T. Miller, *AIChE J.*, 2003, **49**, 1300–1306.
2 B. A. Buffett, *Annu. Rev. Earth Planet. Sci.*, 2000, **28**, 33.
3 E. D. Sloan and C. A. Koh, *Clathrate Hydrates of Natural Gases*, CRC Press, 3rd edn, 2008.
4 P. Englezos and J. D. Lee, *Korean J. Chem. Eng.*, 2005, **22**, 11.
5 C. A. Koh, *Chem. Soc. Rev.*, 2002, **31**, 157–167.
6 Z. R. Chong, S. H. B. Yang, P. Babu, P. Linga and X.-S. Li, *Appl. Energy*, 2016, **162**, 1633–1652.
7 M. Bui, C. S. Adjiman, A. Bardow, E. J. Anthony, A. Boston, S. Brown, P. S. Fennell, S. Fuss, A. Galindo, L. A. Hackett, J. P. Hallett, H. J. Herzog, G. Jackson, J. Kemper, S. Krevor, G. C. Maitland, M. Matuszewski, I. S. Metcalfe, C. Petit, G. Puxty, J. Reimer, D. M. Reiner, E. S. Rubin, S. A. Scott, N. Shah, B. Smit, J. P. M. Trusler, P. Webley, J. Wilcox and N. Mac Dowell, *Energy Environ. Sci.*, 2018, **11**, 1062–1176.
8 J. J. Zheng, Z. R. Chong, M. F. Qureshi and P. Linga, *Energy Fuels*, 2020, **34**, 10529–10546.
9 H. P. Veluswamy, A. Kumar, Y. Seo, J. D. Lee and P. Linga, *Appl. Energy*, 2018, **216**, 262–285.
10 B. Tohidi, J. H. Yang, M. Salehabadi, R. Anderson and A. Chapoy, *Environ. Sci. Technol.*, 2010, **44**, 1509–1514.
11 C. G. Xu, X. S. Li, K. F. Yan, X. K. Ruan, Z. Y. Chen and Z. M. Xia, *Chin. J. Chem. Eng.*, 2019, **27**, 1998–2013.
12 F. G. Li, Q. Yuan, T. D. Li, Z. Li, C. Y. Sun and G. J. Chen, *Chin. J. Chem. Eng.*, 2019, **27**, 2062–2073.
13 D. Y. Koh, H. Kang, J. W. Lee, Y. Park, S. J. Kim, J. Lee, J. Y. Lee and H. Lee, *Appl. Energy*, 2016, **162**, 114–130.
14 J. M. Schicks, B. Strauch, K. U. Heeschen, E. Spangenberg and M. Luzi-Helbing, *J. Geophys. Res.: Solid Earth*, 2018, **123**, 3608–3620.
15 A. Falenty, J. Qin, A. N. Salamatin, L. Yang and W. F. Kuhs, *J. Phys. Chem. C*, 2016, **120**, 27159–27172.
16 X. B. Zhou, F. H. Lin and D. Q. Liang, *J. Phys. Chem. C*, 2016, **120**, 25668–25677.

17 X. B. Zhou, D. L. Li, S. H. Zhang and D. Q. Liang, *Energy*, 2017, **140**, 136–143.
18 J. F. Zhao, L. X. Zhang, X. Q. Chen, Y. Zhang, Y. Liu and Y. C. Song, *Energy Explor. Exploit.*, 2016, **34**, 129–139.
19 Y. H. Sun, G. B. Zhang, S. L. Li and S. H. Jiang, *Chem. Eng. J.*, 2019, 375.
20 A. N. Salamatin, A. Falenty and W. F. Kuhs, *J. Phys. Chem. C*, 2017, **121**, 17603–17616.
21 M. Ota, Y. Abe, M. Watanabe, R. L. Smith and H. Inomata, *Fluid Phase Equilib.*, 2005, **228**, 553–559.
22 M. Ota, K. Morohashi, Y. Abe, M. Watanabe, R. L. Smith and H. Inomata, *Energy Convers. Manage.*, 2005, **46**, 1680–1691.
23 D. Y. Koh, H. Kang, D. O. Kim, J. Park, M. Cha and H. Lee, *Chemsuschem*, 2012, **5**, 1443–1448.
24 C. G. Xu, J. Cai, Y. S. Yu, K. F. Yan and X. S. Li, *Appl. Energy*, 2018, **217**, 527–536.
25 S. Lee, Y. Lee, J. Lee, H. Lee and Y. Seo, *Environ. Sci. Technol.*, 2013, **47**, 13184–13190.
26 S. Lee, S. Park, Y. Lee and Y. Seo, *Chem. Eng. J.*, 2013, **225**, 636–640.
27 G. Ersland, J. Husebo, A. Graue, B. A. Baldwin, J. Howard and J. Stevens, *Chem. Eng. J.*, 2010, **158**, 25–31.
28 M. Uddin and D. Coombe, *J. Phys. Chem. A*, 2014, **118**, 1971–1988.
29 P. Guo, Y.-K. Pan, L.-L. Li and B. Tang, *Chin. Phys. B*, 2017, **26**, 073101.
30 Y. Liu, J. Zhao and J. Xu, *Comput. Theor. Chem.*, 2012, **991**, 165–173.
31 N. J. English and G. M. Phelan, *J. Chem. Phys.*, 2009, **131**, 074704.
32 F. Jiménez-Ángeles and A. Firoozabadi, *J. Phys. Chem. C*, 2014, **118**, 11310–11318.
33 M. R. Walsh, C. A. Koh, E. D. Sloan, A. K. Sum and D. T. Wu, *Science*, 2009, **326**, 1095–1098.
34 L. Y. Ding, C. Y. Geng, Y. H. Zhao and H. Wen, *Mol. Simul.*, 2007, **33**, 1005–1016.
35 J. X. Liu, Y. J. Yan, H. Y. Liu, J. F. Xu, J. Zhang and G. Chen, *Chem. Phys. Lett.*, 2016, 648.
36 Y. T. Tung, L. J. Chen, Y. P. Chen and S. T. Lin, *J. Phys. Chem. B*, 2011, **115**, 15295–15302.
37 D. S. Bai, X. R. Zhang, G. J. Chen and W. C. Wang, *Energy Environ. Sci.*, 2012, **5**, 7033–7041.
38 G. Z. Wu, L. Q. Tian, D. Y. Chen, M. Y. Niu and H. Q. Ji, *J. Phys. Chem. C*, 2019, **123**, 13401–13409.
39 S. Sarupria and P. G. Debenedetti, *J. Phys. Chem. A*, 2011, **115**, 6102–6111.
40 Y. Qi, W. Wu, Y. Liu, Y. Xie and X. Chen, *Fluid Phase Equilib.*, 2012, **325**, 6–10.
41 L. Yi, D. Liang, X. Zhou, D. Li and J. Wang, *Mol. Phys.*, 2014, **112**, 3127–3137.
42 Z. He, P. Linga and J. Jiang, *Phys. Chem. Chem. Phys.*, 2017, **19**, 15657–15661.
43 J. L. F. Abascal and C. Vega, *J. Chem. Phys.*, 2005, **123**, 234505.
44 Z. G. Zhang and Z. H. Duan, *J. Chem. Phys.*, 2005, **122**, 214507.
45 M. P. Allen and D. J. Tildesley, *Computer Simulation of Liquids*, Oxford University PresS, New York, 1987.
46 G. Makov and M. C. Payne, *Phys. Rev. B: Condens. Matter Mater. Phys.*, 1995, **51**, 4014–4022.
47 T. Darden, D. York and L. Pedersen, *J. Chem. Phys.*, 1993, **98**, 10089–10092.
48 G. J. Guo, Y. G. Zhang, C. J. Liu and K. H. Li, *Phys. Chem. Chem. Phys.*, 2011, **13**, 12048–12057.
49 P. M. Rodger, T. R. Forester and W. Smith, *Fluid Phase Equilib.*, 1996, **7**(116), 326–332.
50 Z. Y. Yin, M. Khurana, H. K. Tan and P. Linga, *Chem. Eng. J.*, 2018, **342**, 9–29.
51 L. Z. Yi, X. B. Zhou, Y. B. He, Z. D. Cai, L. L. Zhao, W. K. Zhang and Y. Y. Shao, *J. Phys. Chem. B*, 2019, **123**, 9180–9186.
52 L. Z. Yi, D. Q. Liang, X. B. Zhou, D. L. Li and J. W. Wang, *Mol. Phys.*, 2014, **112**, 3127–3137.
53 C. Holzammer, A. Finckenstein, S. Will and A. S. Braeuer, *J. Phys. Chem. B*, 2016, **120**, 2452–2459.
54 G. J. Guo and P. M. Rodger, *J. Phys. Chem. B*, 2013, **117**, 6498–6504.
55 Z. Zhang, P. G. Kusalik and G. J. Guo, *Phys. Chem. Chem. Phys.*, 2018, **20**, 24535–24538.